Towards an Adaptive Minimum Variance Control Scheme for Specimen Drift Compensation in Transmission Electron Microscopes

Arturo Tejada*, Pauline Vos and Arnold J. den Dekker

Abstract— **Transmission electron microscopes are the tools of choice in materials science, semiconductor, and biological research and it is expected that they will be increasingly used to autonomously perform high-volume, repetitive, nano-measurements in the near future. Thus, there is a clear need to develop automation strategies for these microscopes.**

This paper introduces an adaptive minimum variance control scheme to compensate specimen drift, a common cause of image blurring in long-exposure images. The controller, which is new in the electron microscope literature, makes use of ARMASA, a statistical toolbox designed to identify linear models from finite-length data sets, to generate ARMA models of the drift process 'on-the-fly'. These models are then used as part of a controller designed to reduce the drift variance. The benefits of the proposed scheme, which can be quite substantial, are illustrated through a set of simulations that use a model of the drift present in a sequence of experimental images.

I. Introduction

Transmission electron microscopes (TEMs) are the tools of choice in materials science, semiconductor, and biological research because they can reveal information on the internal structure of a wide range of specimens. In the near future, TEMs will be increasingly used to perform high-volume, repetitive measurements in industrial settings (such as those required for quality control in semiconductors production lines). Thus, there is need of a new generation of TEMs capable of autonomously performing and reporting high-throughput nano-scale measurements. As was recently suggested, such TEMs could be developed with the aid of systems and control concepts [1].

An important TEM process in need of automation is that of specimen drift compensation. Specimen drift is present in all types of electron microscopes and is caused by specimen charging, electromagnetic interference, relaxation of the specimen transporting mechanism (i.e., the specimen holder), thermal changes, and other factors [2], [3], [4]. At low magnification, it causes a slow shift of the content in the microscope's image stream. At high magnification, this shift is much more pronounced and can potentially lead to image blurring, specially for long-exposure TEM images [2], or to image distortions [5]. Specimen drift can be ameliorated by hosting the microscope in a specially-conditioned laboratory [4] and by carefully setting up the experimental conditions under which the images are acquired [2]. The latter requires one to allow the microscope to reach thermal and mechanical equilibria by waiting several minutes (sometimes hours) before acquiring the images. Unfortunately, such preventive procedures are not compatible with high-throughput microscope operation. An alternative is to use image restoration techniques to remove the effect of the drift (see, e.g.,[6], [7], [5]). Although these techniques yield good results, they are not able to prevent the blurring of long-exposure images. Feedback control schemes without the necessary prediction capabilities (see, e.g., [8]), present a similar disadvantage.

To address this problem, this paper presents an adaptive minimum variance (AMV) control scheme for specimen drift compensation that, to the best of our knowledge, is new to the electron microscopy community. The scheme employs an auto-regressive moving average (ARMA) model of the specimen drift process to forecast and compensate drift values. In contrast with recent related work in the atomic force microscope literature [9], the drift model is not assumed to be known a-priori. Instead, it is identified directly from measured drift data using the ARMASA toolbox for Matlab [10], [11]. Clearly, this approach provides the compensation mechanism with the ability to adapt to changing drift properties, since the ARMA model is updated with every new drift measurement. This model, in turn, is used to predict future drift values using standard minimum mean square error predictors (e.g, a Kalman filter). This scheme is an alternative to those in [12], [13] and aims to reduce the variance of the shift in the image stream content over time.

The rest of the document is organized as follows: Section II summarizes the operation of a TEM microscope, emphasizing the actuators available for drift compensation. Section III presents the AMV control (AVMC) scheme, while Section IV provides an illustrative example. Finally, our conclusions are stated in Section V.

II. Fundamentals of TEM Operation

A detailed description of the TEM principle of operation can be found in, for example, [14], [15]. Here, only a brief summary of the formation of the so-called amplitude contrast bright-field images, an important type of TEM images, is offered (see Figure 1): A TEM uses an electron beam as its illumination source. The electron source has finite width, so it is first demagnified by a set of condenser lenses (CL) to obtain an almost ideal point source. The demagnified source lays at the front focal plane of the upper portion of the objective lens (UOL), which is the main lens in a TEM. This lens ensures that the specimen under inspection is illuminated by a uniform parallel electron beam. The electrons that go through the specimen are collected by the lower portion of

The authors are with the Delft Center for Systems and Control (DCSC), Delft University of Technology, The Netherlands. *Corresponding author: a.tejadaruiz@tudelft.nl

978-1-61284-817-4/11/$26.00 ©2011 IEEE

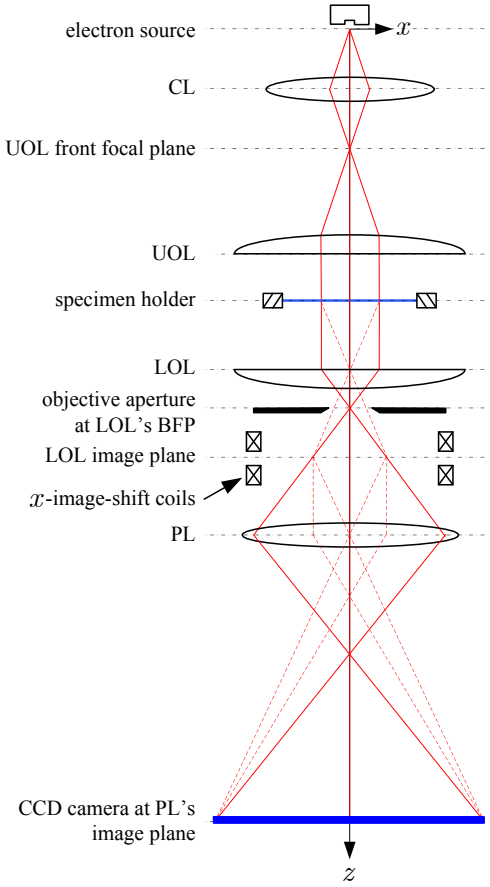

Fig. 1. Main TEM components and amplitude-contrast, bright-field image formation.

the objective lens (LOL) and used to form an image of the specimen at the LOL's image plane. This image is in turn magnified and projected on a CCD camera, which records the images, by a set of projection lenses (PL).

The contrast in these images is determined by the atomic weight of the atoms conforming the specimen and by the presence of the objective aperture: Heavier atoms scatter electrons at higher flight angles than lighter ones. Electrons at higher angles are focused by the LOL at its back focal plane (BFP) away from the z-axis (the so-called optical axis). Thus, a small, round objective aperture is placed at this plane and centered at the optical axis to allow only the lightly scattered and un-scattered electrons to go through and contribute to the images. Thus, the resulting images present darker areas where more heavy atoms are located in the specimen.

Finally, note from Figure 1 that the portion of the specimen visible at the CCD camera can be adjusted by displacing either the specimen or the image at the LOL's image plane relative to the optical axis. The specimen position is adjusted by means of a specimen holder, which is able to position the specimen in three-dimensional space by means of motor actuation. The holder provides a motion range of several millimeters, with an accuracy of around a hundred nanometers [16], and is primarily used for long-range translation of the specimen. On the other hand, the position of the image at the LOL's image plane is adjusted by electronic means using two sets of image-shift coils (see Figure 1). Although their shift range is more limited than that of the specimen holder, these coils provide a faster and finer mean of adjusting what the camera sees. Thus, the image-shift coils are the actuators of choice for short-range specimen drift compensation, and our proposed AMVC scheme relies on them. The details of our scheme are presented next.

III. An ARMASA-Based AMVC Scheme

This section is divided in three subsections: The first one describes the main elements of the AMVC scheme and states its assumptions, the second one presents the standard modeling and forecasting techniques for ARMA processes, and the last part one provides the details of the AMV controller.

A. Model Assumptions and Description

Specimen drift is manifested by an undesired translation of the image content (specimen drift in the z-axis direction is considered elsewhere [17]). Since the adjustments to the image content provided by either the image-shift coils or the specimen holder are indistinguishable from each other, it will be assumed that the specimen's position is constant; that the position with respect of the optical axis, $\boldsymbol{r}(k) \in \mathbb{R}^2$, $k \in \mathbb{N}^1$, of the content in the k-th image produced by the CCD camera is determined only by the position of the image at the LOL's image plane, $r_b(k) \in \mathbb{R}^2$, set by the image-shift coils; and that the drift is a stationary stochastic process that acts as an additive perturbation, $\boldsymbol{d}(k)$, to the aforementioned position. Thus,

$$\boldsymbol{r}(k) = r_b(k) + \boldsymbol{d}(k).$$

Under these assumptions, the proposed AMVC scheme can be modeled as shown in Figure 2. In this figure, $I(k) \in \mathbb{R}^{n \times n}$, $n \in \mathbb{N}^+$, denotes the k-th image produced by the camera, which is assumed to be recorded under constant $r_b(k)$ and drift value $\boldsymbol{d}(k)$. The latter is equivalent to assuming that the image exposure time is short compared to the drift rate. This is a valid assumption for short exposure images (100 ms or less), since the usual specimen drift rates of 0.12 nm/min to 0.5 nm/s (see [18], [4]) yield less than 1 pixel displacement at the typical magnification scale of 1 Å/pixel. The assumption that $r_b(k)$ remains constant during image acquisition is justified by the speed of modern deflection coils, which can reach steady responses in just a few microseconds (see, e.g., [19]). Thus, in the sequel, it will be assumed that the image-shift coils present no dynamics. Moreover, without loss of generality, it will be assumed that $r_b(k) \equiv u(k)$, where $u(k)$ is the commanded image-shift position.

As shown in Figure 2, specimen drift is estimated by measuring the relative displacement of the content in each image, $I(k)$, with respect to the content in a *fixed* reference

[1]Random variables and processes are denotes in boldfaced fonts, $\mathbb{N}$ denotes the non-negative integers, and $\mathbb{N}^+$ denotes the positive integers.

978-1-61284-817-4/11/$26.00 ©2011 IEEE

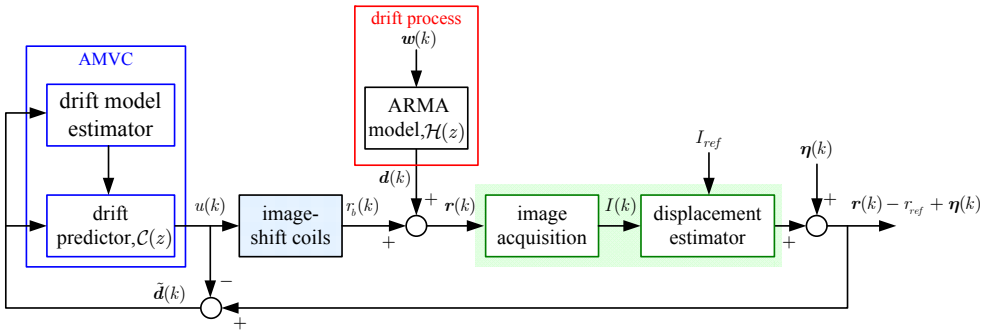

Fig. 2. Main elements of the proposed adaptive minimum variance control scheme for drift compensation.

image, I_{ref}. This is done by using image processing techniques such as phase-correlation or cross-correlation [8], [12] (different techniques are needed to measure drift in the z-axis direction [17], [20]) . Since the interest here is on $\boldsymbol{d}(k)$, the known value $r_b(k) = u(k)$ could be subtracted from the aforementioned displacement to produce the drift estimate, $\tilde{\boldsymbol{d}}(k)$, given by

$$\tilde{\boldsymbol{d}}(k) = \boldsymbol{d}(k) - r_{ref} + \boldsymbol{\eta}(k), \tag{1}$$

where r_{ref} is the (probably unknown) position, with respect of the optical axis, of the content in the reference image, and $\boldsymbol{\eta}(k) \in \mathbb{R}^2$ is a Gaussian white noise process, with covariance matrix $\Sigma_\eta = \text{diag}(\sigma_\eta^2, \sigma_\eta^2)$, that models the displacement measurement error.

Finally, as in [12], it will be assumed that the drifts in the x and y directions are independent. It follows from this that the same analysis and drift compensation techniques can be applied independently in each spatial direction. Thus, with a slight abuse of notation, we will write $\boldsymbol{r}(k)$, $r_d(k)$, $u(k)$, $\boldsymbol{d}(k)$, $\boldsymbol{\eta}(k)$, and $\tilde{\boldsymbol{d}}(k)$ instead of $\boldsymbol{r}_x(k)$, $r_{d_x}(k)$, $u_x(k)$, $\boldsymbol{d}_x(k)$, $\boldsymbol{\eta}_x(k)$, and $\tilde{\boldsymbol{d}}_x(k)$ (or $\boldsymbol{r}_y(k)$, $r_{d_y}(k)$, $u_y(k)$, $\boldsymbol{d}_y(k)$, $\boldsymbol{\eta}_y(k)$, and $\tilde{\boldsymbol{d}}_y(k)$). Note, however, that the ideas proposed here can be extended to the case where the x and y drifts are dependent by using vector ARMA identification techniques.

B. Modeling and Forecasting Drift via ARMA Techniques

Under the stationarity assumption, the drift can be modeled as an ARMA(p, q) process [21], [22]. That is,

$$\phi(B)\boldsymbol{d}(k) = \theta(B)\boldsymbol{w}(k), \tag{2}$$

where $\phi(B) = 1 - \sum_{i=1}^{p} \phi_i B^i$ and $\theta(B) = 1 - \sum_{i=1}^{q} \theta_i B^i$ are, respectively, p and q order polynomials on B, the backward shift operator (i.e., $B\boldsymbol{d}(k) = \boldsymbol{d}(k-1)$), and $\boldsymbol{w}(k)$ is a zero-mean white noise process with variance σ_w^2. In addition, without loss of generality (see below), it will be assumed that $\boldsymbol{w}(k)$, and thus $\boldsymbol{d}(k)$, have zero mean. Note from the stationarity of $\boldsymbol{d}(k)$ that the roots of $\phi(B)$ must lie outside the unitary circle on the complex plane [22]. Thus, (2) defines a stable discrete-time, linear, time-invariant system with discrete-time transfer function, $\mathcal{H}(z)$, given by

$$\mathcal{H}(z) = \frac{\theta(z^{-1})}{\phi(z^{-1})} = \psi(z^{-1}),$$

where $\psi(z^{-1}) = 1 + \sum_{i=1}^{\infty} \psi_i z^{-i} = \phi^{-1}(z^{-1})\theta(z^{-1})$. It follows from this that the drift variance, σ_d^2, is given by [22]

$$\sigma_d^2 = \sigma_w^2 \sum_{i=0}^{\infty} \psi_i^2 > \sigma_w^2. \tag{3}$$

Given data points $\{\boldsymbol{d}(0), \ldots, \boldsymbol{d}(k)\}$, the minimum mean square error forecast, $\hat{\boldsymbol{d}}(k, l)$, of $\boldsymbol{d}(k + l)$, $l = 1, 2, \ldots$, can be found by solving the recursion [22]

$$\hat{\boldsymbol{d}}(k, l) = \sum_{i=1}^{p} \phi_i \hat{\boldsymbol{d}}(k, l - i) - \sum_{i=l}^{q} \theta_i \boldsymbol{w}(k + l - i), \tag{4}$$

where $\hat{\boldsymbol{d}}(k, l-i)$ is replaced by the recorded value $\boldsymbol{d}(k+l-i)$ for $l - i \leq 0$ and the right-most summation vanishes for $l > q$. Note that this recursion can be solved iteratively or by first transforming it into a state-space model and then using Kalman filtering techniques [22]. In either case, the variance of the forecast error, $\boldsymbol{e}(k, l) \triangleq \boldsymbol{d}(k + l) - \hat{\boldsymbol{d}}(k, l)$, is given by

$$\text{Var}\{\boldsymbol{e}(k, l)\} = \sigma_w^2 \sum_{i=0}^{l-1} \psi_i^2 \leq \sigma_d^2. \tag{5}$$

As will be shown in Subsection C, the latter inequality is the basis of the AMVC method.

Now, let $\mu_{\tilde{d}}$ represent the mean of $\tilde{\boldsymbol{d}}(k)$. Thus, it follows from (1) that $\mu_{\tilde{d}} = -r_{ref}$. Moreover, it follows from (2) that [22]

$$\begin{aligned} \phi(B)(\tilde{\boldsymbol{d}}(k) - \mu_{\tilde{d}}) &= \theta(B)\boldsymbol{w}(k) + \phi(B)\boldsymbol{\eta}(k) \\ &= \vartheta(B)\boldsymbol{\varpi}(k), \end{aligned} \tag{6}$$

where $\vartheta(B) = 1 - \sum_{i=1}^{Q} \vartheta_i B^i$, $Q = \max\{p, q\}$, and $\boldsymbol{\varpi}(k)$ is a zero-mean, white noise process with variance σ_{ϖ}^2 larger than both σ_w^2 and σ_η^2. Observe from (6) that in the absence of measurement noise, the ARMA transfer function $\mathcal{H}(z)$ can be identified directly from the de-trended data, $\tilde{\boldsymbol{d}}(k) - \mu_{\tilde{d}}$. De-trending $\tilde{\boldsymbol{d}}(k)$ can be done systematically (see, e.g., [10], [23]) and removes not only r_{ref} but also the (possibly polynomial) trend that $\boldsymbol{d}(k)$ presents in practice. That is, in practice $\boldsymbol{d}(k)$ may not be stationary (an example of such behavior, obtained from a sequence of experimental TEM images, is shown in Figure 3). Once an estimate of the model, $\hat{\mathcal{H}}(z)$, has been produced, it can be used to forecast future

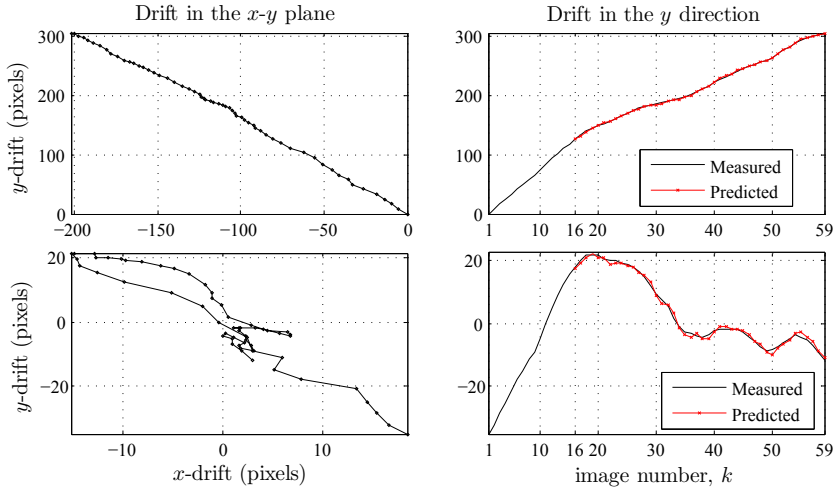

Fig. 3. Top left: x-y plane specimen drift present in a TEM bright-field image sequence recorded with a TEM Tecnai F20[2]. The drift has a clear linear trend from the bottom right to the upper left (the dots mark the recorded data points). Bottom left: De-trended x-y drift data. Top right: y-direction drift and the one-step forecast sequence generated with ARMAsel and ARMApred (doted line). Bottom right: De-trended y-direction drift and its one-step forecast sequence. In both cases, the first drift forecast is $\hat{\boldsymbol{d}}(15,1)$.

values of the de-trended process, $\tilde{\boldsymbol{d}}(k)-\mu_{\tilde{d}}$. The latter can in turn be used to forecast $\boldsymbol{d}(k)$ by re-introducing the removed trend. Thus, there is no loss of generality in assuming, as done above, that $\boldsymbol{d}(k)$ is a zero-mean stationary process, nor by assuming that $r_{ref}=0$, as will be done in the sequel.

Model identification can be performed with a number of methods. Here, the modified Durbin method advocated in [21] is used, since it is designed to minimize the model identification error using finite data sets. This method is capable of autonomously selecting the model order, p, and estimating the parameters of the ARMA$(p,p-1)$ model that best fits the data, when at least $10p$ data points are available. More importantly, the identified model is guaranteed to be both stable and invertible (i.e., both the poles and zeros of $\hat{\mathcal{H}}(z)$ lie inside the unitary circle, which, as shown in the next subsection, is important for control purposes). This method, called ARMAsel, is available in the ARMASA toolbox for Matlab [10], [11]. ARMASA also contains a data forecasting tool, ARMApred, which generates $\hat{\boldsymbol{d}}(k,l)$ based on the techniques described in [24], [25].

Finally, note that in the presence of measurement noise, ARMAsel will return an estimated transfer function, $\hat{\mathcal{H}}(z)$, whose numerator is closer to $\vartheta(z^{-1})$ than to $\theta(z^{-1})$. Thus, it follows from (3), (5), and (6) that $\mathrm{Var}\{\boldsymbol{e}(k,l)\}$ increases as σ_η^2 does. This is explored further in Section IV.

C. AMVC based on ARMAsel and ARMApred

The proposed AMVC scheme is a variation of the one proposed by Åström in [26]:

AMVC Algorithm 1: After acquiring the k-th image

1) Compute $\tilde{\boldsymbol{d}}(k)$ and generate an estimate $\hat{\mathcal{H}}(k)$ of $\mathcal{H}(k)$ using the recorded data $\{\tilde{\boldsymbol{d}}(0),\ldots,\tilde{\boldsymbol{d}}(k)\}$ and ARMAsel.
2) Using $\hat{\mathcal{H}}(k)$ and ARMApred compute $\hat{\boldsymbol{d}}(k,1)$ and set $u(k+1)=-\hat{\boldsymbol{d}}(k,1)$.

Note from (2) and (4) that if $\hat{\mathcal{H}}(z)$ and $\mathcal{H}(z)$ were equal, then

$$\begin{aligned} u(k+1) &= -\hat{\boldsymbol{d}}(k,1) \\ &= -\sum_{i=1}^{p}\phi_i\boldsymbol{d}(k+1-i)+\sum_{i=1}^{q}\theta_i\boldsymbol{w}(k+1-i) \\ &= (\phi(B)-1)\boldsymbol{d}(k+1)+(1-\theta(B))\boldsymbol{w}(k+1) \\ &= -\boldsymbol{d}(k+1)+\boldsymbol{w}(k+1). \end{aligned} \tag{7}$$

So, in the absence of measurement noise $\boldsymbol{r}(k+1)=u(k+1)+\boldsymbol{d}(k+1)=\boldsymbol{w}(k+1)$. This would clearly reduce the variance of the *image content drift*. This reduction, however, would become less significant in the presence of strong measurement noise (see previous subsection). Further note that restating (7) as follows

$$u(k+1)=B^{-1}(1-\theta(B))\boldsymbol{w}(k)-B^{-1}(1-\phi(B))\boldsymbol{d}(k)$$

yields after using (2) and multiplying both sides by $B\theta(B)$

$$\begin{aligned} \theta(B)u(k) &= (1-\theta(B))\phi(B)\boldsymbol{d}(k)-(1-\phi(B))\theta(B)\boldsymbol{d}(k) \\ &= -\left(\theta(B)-\phi(B)\right)\boldsymbol{d}(k). \end{aligned}$$

It follows from this that in step 2 of AMVC Algorithm 1, the discrete time transfer function from $\boldsymbol{d}(k)$ to $u(k)$ is given by $-(1-\hat{\mathcal{H}}^{-1}(z))$. Moreover, since $\hat{\mathcal{H}}(z)$ is always invertible (see previous subsection), the proposed AMVC Algorithm 1 is guaranteed to be stable.

It is implicit in the aforementioned algorithm that the images are recorded with the same (short) exposure time. If, however, the $k+1$-th image were to be recorded with an N times longer exposure, the measurements $\{\tilde{\boldsymbol{d}}(k+1),\ldots,\tilde{\boldsymbol{d}}(k+N)\}$ would no longer be available. Nevertheless, since the control system can be made aware of an upcoming long-exposure image (by using the camera

[2]The image sequence was recorded by Dr. Richard M. P. Doornbos (Embedded Systems Institute) and is available at http://www.tejadaruiz.net/nds2011/nds2011-imseq.zip

978-1-61284-817-4/11/$26.00 ©2011 IEEE

shutter signals), the specimen drift can still be ameliorated by executing the following control algorithm:

AMVC Algorithm 2: After acquiring the k-th short exposure image

1) Compute $\tilde{\boldsymbol{d}}(k)$ and generate an estimate $\hat{\mathcal{H}}(k)$ of $\mathcal{H}(k)$ using the recorded data $\{\tilde{\boldsymbol{d}}(0), \ldots, \tilde{\boldsymbol{d}}(k)\}$ and ARMAsel.
2) Using $\hat{\mathcal{H}}(k)$ and ARMApred, compute $\hat{\boldsymbol{d}}(k,1)$ and set $u(k+1) = -\hat{\boldsymbol{d}}(k,1)$.

If the $k+1$-th image is an N times longer exposure image:

3) Using $\hat{\mathcal{H}}(k)$ and ARMApred compute $\hat{\boldsymbol{d}}(k,l)$ and set $u(k+l) = -\hat{\boldsymbol{d}}(k,l)$ for $l = 2, \ldots, N$.
4) Update the recorded data set so it becomes $\{\tilde{\boldsymbol{d}}(0), \ldots, \tilde{\boldsymbol{d}}(k), \hat{\boldsymbol{d}}(k,1), \ldots, \hat{\boldsymbol{d}}(k,N)\}$.
5) Treat the upcoming short exposure image as image $k+N+1$.

In light of (5), it is clear that this algorithm ameliorates the consequences of specimen drift (i.e., blurring) in long exposure images. Since steps 3 to 5 are only executed sporadically (i.e., randomly), the stability of AMVC Algorithm 2 is difficult to establish using standard tools, so it will be analyzed elsewhere (see [27]). The benefits of Algorithm 1 are illustrated next.

IV. An Illustrative Example

Consider again the TEM bright-field image sequence from Figure 3. Using the first image in the sequence as the reference image and a cross-correlation algorithm to compute $\tilde{\boldsymbol{d}}(k)$, $k = 1, \ldots, 59$, it was found using ARMAsel that the de-trended y-direction drift can me modeled with an ARMA(2,1) model, with transfer function

$$\mathcal{H}(z) = \frac{1 - 0.1186z^{-1}}{1 - 1.914z^{-1} + 0.94z^{-2}}. \tag{8}$$

It follows from (3) and from the above equation that in the absence of measurement noise, $\sigma_d = 15.86\sigma_w$ (see (3)). Thus, Algorithm 1 has the potential to significantly reduce the image content. To show this, 500 sample paths of $\boldsymbol{d}(k)$ were simulated using (8) and $\sigma_w = 1$, for $k = 0, \ldots, 200$. The AMCV Algorithm 1 was then applied to each sample path, and the standard deviation of $\boldsymbol{r}(k)$ was computed for each $k \geq 16$ (for $k \leq 15$, ARMAsel does not have enough data points to produce reliable results). Moreover, four noise powers were considered: $\sigma_\eta^2 = 0$, 1, 4, and 10. The results are shown in Figure 4. For comparison purposes, Figure 4 also presents the results of the standard minimum variance control algorithm, which assumes perfect knowledge of the transfer function in (8). Clearly, the drift reduction is significant with both techniques, even when strong measurement noise is present. Although AMVC Algorithm 1 takes longer to reduce the drift variance, it does so without any a-priori information about $\mathcal{H}(z)$. Moreover, it stops being effective only for large measurement noise powers.

It was also clear from these experiments that for strong non-stationary drift processes, the control signal, $u(k)$, can become large enough to exceed the actuation range of the image-shift coils. Note, however, that the specimen drift

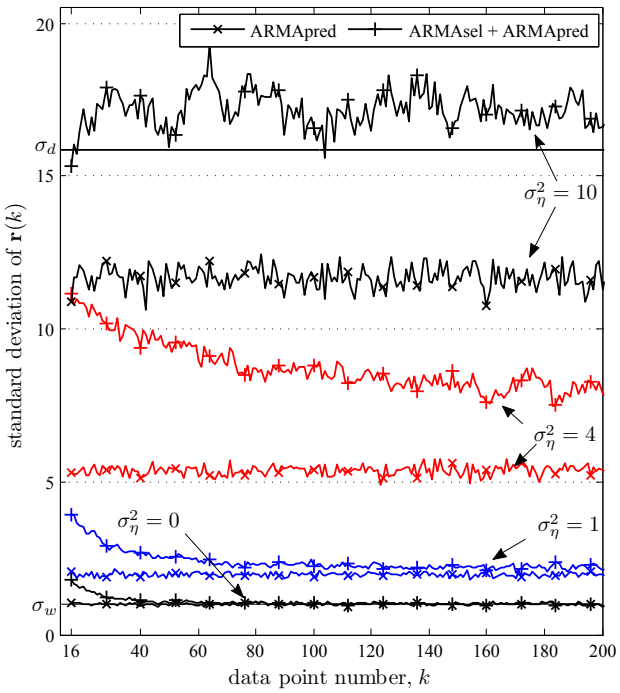

Fig. 4. Standard deviation of $\boldsymbol{r}(k)$ when the AMVC Algorithm 1 (ARMAsel and ARMApred) is applied to 500 simulated sample paths of the ARMA(2,1) process (8) with $\sigma_w^2 = 1$ (+ markers). Four noise powers are considered ($\sigma_\eta^2 = 0$, 1, 4, and 10). For comparison purposes the results of the standard MVC algorithm (only ARMApred), which assumes perfect knowledge of the ARMA(2,1) model, are included ($\times$ markers).

generally subsides over time by itself [2], so the aforementioned limitation also becomes less significant over time. Nevertheless, to avoid the use of large control signals, the AMV controller could be supplemented with, for instance, an H_2 (or an H_∞) controller, which could also provide additional robustness against model estimation errors caused by measurement noise.

V. Conclusions

Specimen drift is an undesired phenomenon that affects all types of electron microscopes and can lead to blurring of long-exposure images. An adaptive minimum variance control scheme, new to the electron microscopy community, was introduced as a potential solution for this problem. The benefits of this approach were explored through simulations, which demonstrated a significant reduction of drift variance even in face of strong measurement noise. Research is ongoing to extend this approach by supplementing it with an H_2 (or an H_∞) controller and to better understand its benefits for long-exposure images.

Acknowledgements

This research was sponsored by the Condor project at FEI company, under the responsibilities of the Embedded Systems Institute (ESI). This project is partially supported by the Dutch Ministry of Economic Affairs under the BSIK program. The authors also acknowledge the instructive technical discussions on control theory held with Ir. Stefan Kuiper and

Dr. Xavier Bombois at DCSC, the insights on TEM imaging provided by Dr. Wouter Van den Broek (EMAT, University of Antwerp), the technical discussions on ARMASA with Dr. Piet M.T. Broersen, and the support of Dr. Richard Doornbos (Embedded Systems Institute) and Dr. Seyno Sluyterman (FEI Company) in the collection of the image sequence used in this work.

REFERENCES

[1] A. Tejada, A. J. den Dekker, and W. Van Den Broek, "Introducing measure-by-wire, the systematic use of systems and control theory in transmission electron microscopy," *Ultramicroscopy*, 2011, to appear.

[2] J. C. H. Spence, *High-Resolution Electron Microscopy, 3rd. Edition*. New York: Oxord University Press, 2003.

[3] J. M. Howe, "In-situ HRTEM studies of interface dynamics during solid-solid phase transformations in metal alloys," in *In-Situ Electron Microcopy at High-Resolution*, F. Banhart, Ed. World Scientific, 2008.

[4] H. Inada, H. Kakibayashi, S. Isakozawa, T. Hashimoto, T. Yaguchi, and K. Nakamura, "Hitachi's development of cold-field emission scanning transmission electron microscopes," in *Cold Field Emission and the Scanning Transmission Electron Microscope*, ser. Advances in Imaging and Electron Physics, P. W. Hawkes, Ed. Elsevier, 2009, vol. 159, pp. 123 – 186.

[5] M. T. Snella, "Drift correction for scanning-electron microscopy," Master's thesis, Massachusetts Institute of Technology, 2010.

[6] J. M. Plitzko and J. Mayer, "Quantitative thin film analysis by energy filtering transmission electron microscopy," *Ultramicroscopy*, vol. 78, no. 1-4, pp. 207 – 219, 1999.

[7] W. Sigle, S. Krämer, V. Varshney, A. Zern, U. Eigenthaler, and M. Rhle, "Plasmon energy mapping in energy-filtering transmission electron microscopy," *Ultramicroscopy*, vol. 96, no. 3-4, pp. 565 – 571, 2003.

[8] R. Tsuneta, M. Koguchi, K. Nakamura, and A. Nishida, "A specimen-drift-free EDX mapping system in a STEM for observing two-dimensional profiles of low dose elements in fine semiconductor devices," *Journal of Electron Microscopy*, vol. 51, no. 3, pp. 167–171, 2002.

[9] B. Mokaberi and A. A. G. Requicha, "Drift compensation for automatic nanomanipulation with scanning probe microscopes," *IEEE Trans. Autom. Sci. Eng.*, vol. 3, no. 3, pp. 199–207, 2006.

[10] P. M. T. Broersen, *Automatic Autocorrelation and Spectral Analysis*. London: Springer-Verlag, 2006.

[11] ——. ARMASA toolbox for Matlab. [Online]. Available: http://www.mathworks.com/matlabcentral/fileexchange/1330

[12] Q. Yang, S. Jagannathan, and E. W. Bohannan, "Automatic drift compensation using phase correlation method for nanomanipulation," *IEEE Trans. Nanotechnol.*, vol. 7, no. 2, pp. 209–216, 2008.

[13] F. Krohs, C. Onal, M. Sitti, and S. Fatikow, "Towards automated nanoassembly with the atomic force microscope: A versatile drift compensation procedure," *Journal of Dynamic Systems, Measurement, and Control*, vol. 131, no. 6, p. 061106, 2009.

[14] D. B. Williams and C. B. Carter, *Transmission Electron Microscopy, A Textbook for Materials Science*. New York: Springer, 2009.

[15] M. De Graef, *Introduction to Conventional Transmission Electron Microscopy*. Cambridge: Cambridge University Press, 2003.

[16] J. Pulokas, C. Green, N. Kisseberth, C. S. Potter, and B. Carragher, "Improving the positional accuracy of the goniometer on the philips CM series TEM," *Journal of Structural Biology*, vol. 128, no. 3, pp. 250 – 256, 1999.

[17] A. Tejada, W. Van Den Broek, S. van der Hoeven, and A. J. den Dekker, "Towards STEM control: Modeling framework and development of a sensor for defocus control," in *Proc. 48th IEEE Conference on Decision and Control*, Shanghai, China, 2009, pp. 8310–8315.

[18] H. Saka, "In-situ high-resolution observation of solid-solid, solid-liquid and solid-gas reactions," in *In-Situ Electron Microcopy at High-Resolution*, F. Banhart, Ed. World Scientific, 2008.

[19] Z. Liu and W. Gu, "High-speed and high-precision deflectors applied in electron beam lithography system based on scanning electron microscopy," *Journal of Vacuum Science & Technology B: Microelectronics and Nanometer Structures*, vol. 22, no. 6, pp. 3557–3559, 2004.

[20] A. Tejada and A. J. den Dekker, "POEM: A fast defocus estimation method for scanning transmission electron microscopy," in *Proc. of the 2011 IEEE International Instrumentation and Measurement Technology Conference*, 2011, pp. 1228–1232.

[21] P. M. T. Broersen, "Automatic spectral analysis with time series models," *IEEE Trans. Instrum. Meas.*, vol. 51, no. 2, pp. 211–216, Apr. 2002.

[22] G. E. P. Box, G. M. Jenkins, and G. C. Reinsel, *Time Series Analysis: Forecasting and Control*. Prentice Hall, 1976.

[23] M. B. Priestley, *Spectral Analysis and Time Series, Vol. 1*. New York: Academic Press, 1981.

[24] R. H. Jones, "Maximum likelihood fitting of ARMA models to time series with missing observations," *Technometrics*, vol. 22, no. 3, pp. 389–395, 1980.

[25] P. Brockwell and R. Davies, *Time Series: Theory and Methods*. New York: Springer Verlag, 1987.

[26] K. J. Åström, *Introduction to Stochastic Control Theory*. New York: Academic Press, 1970.

[27] A. Tejada and J. R. Chávez-Fuentes, "Stability and performance analysis of dual-rate systems with random output rate via Markov jump linear system theory," in *Proc. of the 50th IEEE Conference on Decision and Control*, 2011, under review.